



Self-Organized Macrostructures in Anodically Formed Mesoporous Silica

S. Frey,^{a,b,z} B. Grésillon,^a F. Ozanam,^a J.-N. Chazalviel,^{a,*} J. Carstensen,^b
H. Föll,^{b,*} and R. B. Wehrspohn^{c,*}

^aLaboratoire de Physique de la Matière Condensée, Ecole Polytechnique, 91128 Palaiseau, France

^bFaculty of Engineering, Christian-Albrechts-University of Kiel, 24143 Kiel, Germany

^cPhysik Department, University of Paderborn, 33098 Paderborn, Germany

The electrochemical oxidation of silicon under high potentials (10-30 V) was investigated in weakly alkaline low-buffered fluoride media. The cyclic voltammogram exhibits a hysteresis of several orders of magnitude. Potentiostatically grown oxide films are either pale gray or show thin-film interference colors. Optical spectroscopy indicates here a porous silica layer on a thin compact SiO₂ film. Electron microscopy shows that the brilliant films consist of granular SiO₂ particles with sub-100 nm diameters with a homogeneous film thickness over the etching area. For $U > 15$ V micrometer-sized corrugations lead to a gray appearance. These macrostructures self-organize in a close-packed lattice with narrowly distributed dimensions.
© 2005 The Electrochemical Society. [DOI: 10.1149/1.1960024] All rights reserved.

Manuscript submitted April 6, 2005; revised manuscript received May 3, 2005. Available electronically July 18, 2005.

Porous oxides can be prepared via the sol-gel-process, including porous silica,¹ as well as via electrochemical anodization. In the latter family, the case of Al₂O₃ had been known for more than 50 years,² but it has attracted a lot of attention since it became possible to get ordered structures.^{3,4} TiO₂⁵ has also been shown to exhibit ordered domains, though not yet in the clarity of Al₂O₃, a difference plausibly due to the semiconducting properties of titania.⁶

The extraordinary behavior of p-Si electrodes in acidic fluoride media at anodic potentials has been extensively investigated.^{7,8} Low anodization potentials (< 1-2 V) in aqueous solutions lead to porous silicon structures while larger potentials result in the formation of an anodic oxide layer on the semiconductor electrode which is accompanied (between 3 and 8 V) by pronounced oscillations in current as well as in oxide thickness.⁹ Several models have been invoked to explain these oscillations.¹⁰⁻¹⁴ They more or less survive for potentials up to 20 V.¹⁵ Oscillating behavior under high potential conditions was also reported by Parkhutik et al.¹⁶ for galvanostatic conditions. Above 30 V, water electrolysis leading to oxygen evolution strongly dominates the electrode reactions.¹⁵

The oxide thicknesses produced in nonfluoride media can reach up to several hundred of nanometers by applying voltages of up to 500 V.^{7,8} Beyond that limit, the physical breakdown of the oxide layer prohibits further thickening. In dilute fluoride media, oxide layers of comparable thickness have been observed.¹⁵ Lehmann¹³ reported a change in the morphology of the oxide above a thickness of approximately 10 nm, where the oxide starts to become less dense, i.e., porous. This goes in hand with the transmission electron microscopy (TEM) and scanning electron microscopy (SEM) observations by Aggour et al.,¹⁷ Parkhutik et al.,¹⁶ and Lharch et al.¹⁸ At high voltages, a corrugation of the surface occurs with micrometer-sized depressions.^{16,15} We recently reported on the growth of porous silica films of micrometer thickness at moderate potentials by using a slightly alkaline fluoride electrolyte of low buffer strength.¹⁹ We here report on a preliminary characterization of such films, which turn out to exhibit a variety of morphologies.

Experimental

All experiments were carried out in an EG&G PAR 636 rotating disk electrode setup. The etching cell was a plastic beaker with a Pt-wire loop at the bottom as the counter electrode. Ag/AgCl in saturated KCl with an agarose salt bridge was used as the reference electrode. The potentiostat was custom-built and can supply up to 60 mA and 100 V. The samples were cut from commercially available p-type silicon (100) wafers with a doping of 1–15 Ω cm with a

tempered Au/Al back-side ohmic contact. The electrolytes were NH₄F/NH₃ solutions of low buffer strength with a pH between 8.0-8.5, typically [NH₄F] = 0.1 to 0.3 M and [NH₄F]/[NH₃] = 25. The pH was frequently checked during the experiments. The samples were cut as rectangular pieces and covered with an electrolyte-resistant tape to leave only an etching area of 0.14 cm² for etching on the polished front side. The first experiment with a new electrolyte mixture always consisted of a slow *I*-*V* curve (50 mV/s) to test the system. With a new sample, the potential was first swept from 0 to 25 V at 500 mV/s then backswept at the same speed to the working point, then the sample was maintained under potentiostatic conditions for 10 min. Afterwards the sample was immediately rinsed in deionized water to remove any traces of etching solution. The samples were cleaved and sputtered with nominally 100 Å of Au for better SEM resolution. The SEM images were taken on a Philips XL 40 SEM in plain view as well as at an angle of 60° to get a cross-sectional image. Optical reflectance spectra were taken with a Shimadzu UV-160 spectrophotometer, under 30° incidence angle and using a polished Si surface as reference.

Results

Figure 1 shows the voltammograms for several fluoride concentrations. On the positive potential sweep, the current stays very low as expected for a slightly alkaline fluoride medium (it has been shown earlier that all the characteristic current densities go down by an order of magnitude or more for every ΔpH 1²⁰). After reaching 20 V the current abruptly rises by two orders of magnitude, then keeps increasing with increasing potential, with a nearly constant slope (slope a). This slope is maintained up to approximately 25 V. Above 25 V, heavy bubbling due to oxygen formation starts and the current steeply rises (slope b). When sweeping back the potential, the forward curve is reproduced down to the point where the forward sweep exhibited the strong rise at 20 V. The backward sweep continues with slope a, until the current rapidly drops between 6.5 and 11 V. Slope a is not strongly affected by the fluoride concentration while slope b strongly increases with fluoride concentration (best fitted with a cubic dependence). The onset points for the strong rise (drop) at 20 V (10 V) are not strongly affected by the fluoride concentration, except at the lowest concentrations ($c_F < 0.1$ M), where the hysteresis disappears. The hysteresis behavior is not substantially changed by a slower or larger sweeping speed, only the flanks are smeared out by fast sweeping speeds or become extremely steep in the case of slow sweeping.

Figure 2a-c show the plain and the cross-sectional SEM views after anodizing the sample at 15 V for 10 min in 0.3 M NH₄F/0.012 M NH₃. The resulting anodization current was nearly constant over the whole etching time. The layer itself has a granular morphology. It must be noted that this is not induced by the

* Electrochemical Society Active Member.

^z E-mail: stl@tf.uni-kiel.de

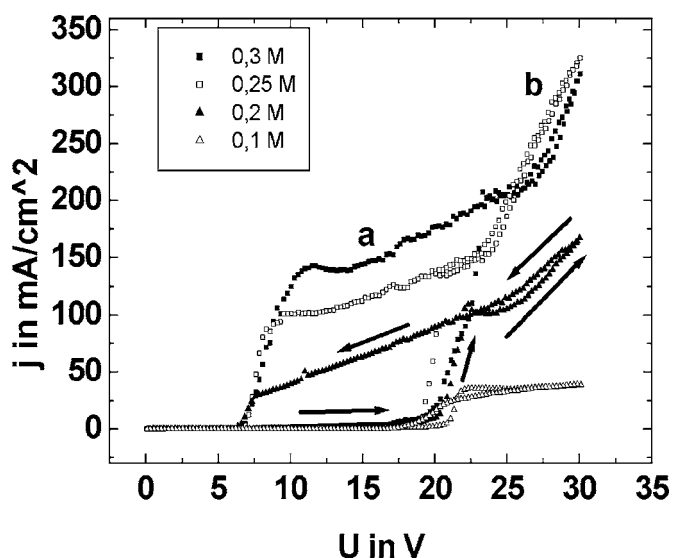


Figure 1. *I-V* curves (scan rate 50 mV/s) for p-type Si(100) in aqueous 0.1...0.3 M $\text{NH}_4\text{F}/0.004...0.012$ M NH_3 ($\text{NH}_4\text{F}:\text{NH}_3$ ratio is always 25:1). The current density exhibits a large hysteresis between the forward and backward scan. Slope a is independent of c_F , while b is strongly dependent on c_F .

Au sputtering prior to the SEM imaging. In a series of sputtering experiments with nominally 2.5, 7, 9, and 18 nm Au thickness, we checked that this morphology is not associated with Au island formation. With 2.5 and 7 nm, the grains were still visible though a little bit blurred due to a lack of conductivity of the layer. With 9 nm an optimal image was obtained, while 18 nm resulted in soft outlines due to a too thick Au layer. On the other hand, a detailed analysis of the grain size was not performed due to the Au sputtering. As the grain size is close to the nominal sputter thickness of 10 nm it would be unjustified to say more about the grain size than that it is between 0 and 50 nm. These layers were also characterized by optical reflectance spectroscopy. Figure 3 shows a typical reflectance curve. Using SCOUT software,²¹ these data can be accounted for by a duplex layer (60 nm compact layer of a composite 6:94 Si: SiO_2 medium, and 400 nm of a porous SiO_2 layer, with a porosity linearly increasing from 50 to 70% at the outer surface). These optical determinations of layer thickness were in fair agreement with the results obtained by direct SEM examination. Figure 2d shows that the thickness of the layer (here SEM data) is a strongly decreasing function of fluoride concentration. At low fluoride concentrations (e.g., 0.2 M), the layer exhibits micrometer sized cracks as shown in Fig. 4. For this case, the thickness of the part of the layer which remains uncracked has been represented in Fig. 2d.

When the anodization potential is increased to 20 V, the layer exhibits dramatic changes. The surface becomes corrugated with micrometer-sized macrobowls (cf. Fig. 5). The macrobowls are covered again with an approximately 500 nm thick layer of granular

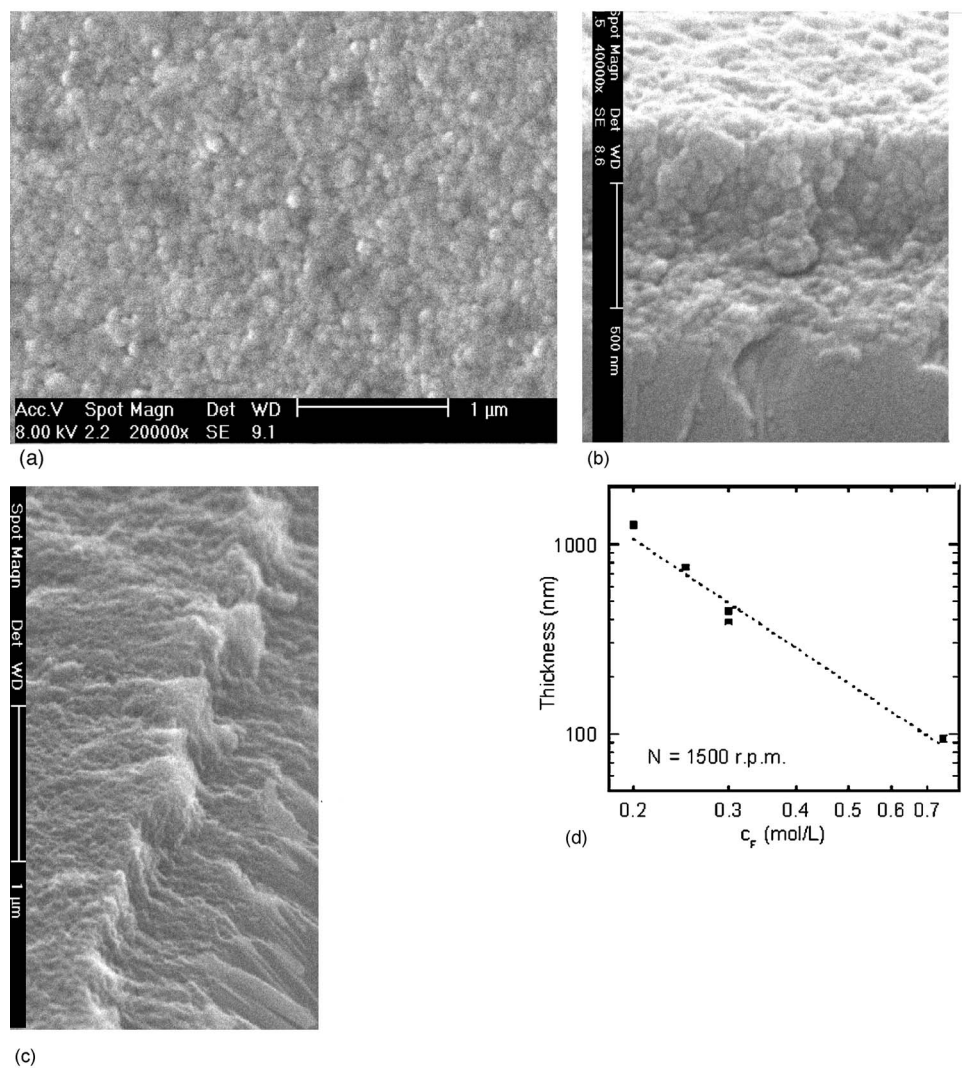


Figure 2. p-Si (100) 2–10 Ω cm anodized in 0.25 M $\text{NH}_4\text{F}/0.01$ M NH_3 for 10 min at $U = \text{const.} = 10$ V, $j = 80...90$ mA/cm². (a) Plain view of the porous anodic oxide layer, (b) tilted cross section (60° to surface normal), (c) rotated cross section. As the substrate cleavage is along a (111) plane, i.e., not perpendicular to the surface, and the layer breaks perpendicular, a step appears at the edge. (d) Thickness vs. fluoride concentration. A significant decay with fluoride concentration is visible. The guide to the eye is a power-law fit corresponding to $c_F^{-1.9}$. For $c_F = 0.2$ M the real layer thickness is much larger (cf. Fig. 4) but only the thickness of the noncracked part was taken for the fit (see also text).

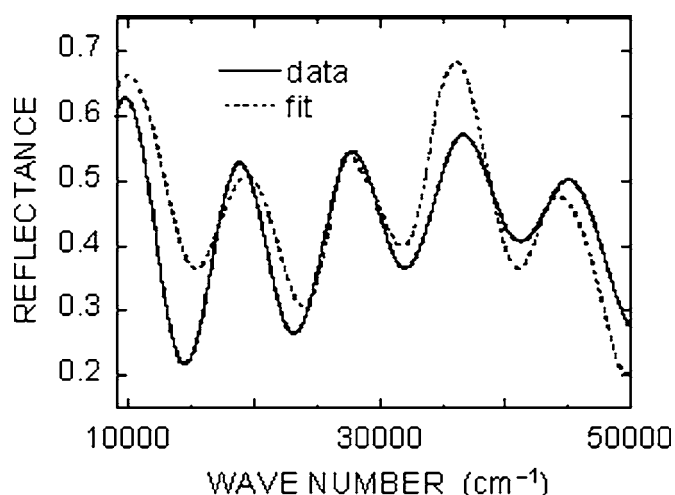


Figure 3. Reflectance of a p-Si (100) sample anodized in 0.25 M $\text{NH}_4\text{F}/0.01$ M NH_3 for 3 min at $U = 15$ V and 500 rpm. The dashed line is a fit to a model featuring a compact inner oxide film and a porous outer film with a porosity gradient.

material. It has to be noted that both interfaces are corrugated (cf. Fig. 5c), i.e., the Si-porSiO₂ interface as well as the SiO₂ surface. Furthermore, the macrostructures exhibit a strong self-ordering. An autocorrelation analysis of Fig. 5a showed that the nearest-neighbor distance is narrowly distributed around 2.0 μm with no global preferential direction.

Discussion

In acidic HF,¹³ a transition of the oxide towards a porous morphology starts as soon as the layer thickness exceeds 11 nm, which is definitely the case at the high voltages considered here. Such a transition is indeed observed, but without significant hysteresis in

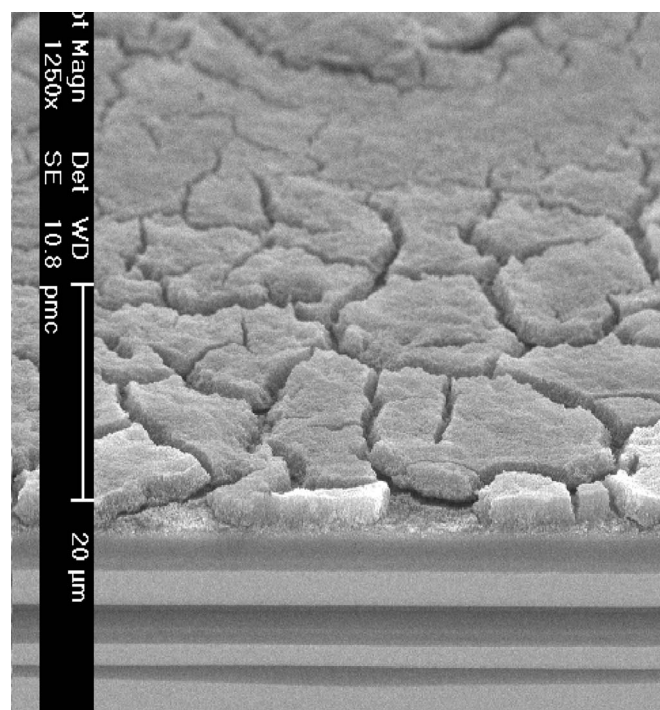
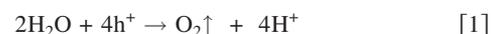


Figure 4. p-Si (100) 2-10 Ω cm anodized in 0.2 M $\text{NH}_4\text{F}/0.008$ M NH_3 for 10 min at $U = \text{const.} = 15$ V. $j = 80\text{--}90$ mA/cm². Tilted cross-sectional SEM view.

the I - V curve.¹⁸ Appearance of a bistable behavior then requires a further ingredient. The upper branch of the I - V curve in Fig. 1a is similar to the behavior observed in acidic fluoride medium.¹⁸ Furthermore the hysteresis is not substantially altered by the sweeping speed, so unlike transient phenomena during potential sweeps like adsorption/desorption or diffusion-controlled redox reactions, this system appears to remain in an activated state once it is triggered. This is in line with the observation that under constant potential conditions the current does not show a substantial decrease even after hundreds of seconds. Together with the earlier observation²⁰ that the current in the Si/HF system can rise by orders of magnitude with decreasing pH, this suggests that the local pH at the electrode becomes acidic when the system jumps to the upper branch. Namely, the medium in the vicinity of the electrode remains weakly alkaline (i.e., with a low current) until a triggering mechanism leads to an acidification near the electrode surface. It is plausible that water electrolysis, which later on leads to heavy bubbling at the electrode (above 25 V), is this triggering process



This assumption is also supported if one extrapolates region b of the I - V curves to zero current. This extrapolation intersects the potential axis at about the potential where the system jumps from the low current to the high current branch, i.e., at around 20 V, suggesting that this is indeed the onset potential for oxygen evolution. Furthermore, the oxide becomes an electronic conductor at these high voltages¹⁵ which makes a water dissociation at the outer oxide interface possible.

Once the system is activated, the created protons can escape only by diffusion, and the medium remains locally acidic even if the potential is lowered below 20 V. We are currently working on a diffusion-oriented modeling to explain the current findings qualitatively and quantitatively.

The overall reactions at the interface can be summarized as follows:

Electrochemical tetravalent oxide formation



and chemical dissolution of the oxide



Reaction 2 leads to a local lowering of the pH while Reaction 3 turns the medium less acidic. This already explains partially why in a weakly alkaline medium oxides are so slowly dissolved. Here the electrolyte was intentionally prepared with a low buffer strength ($[\text{NH}_4^+]/[\text{NH}_3] = 25$). If protons are locally added to such a system the buffer can be rapidly put out of function, i.e., the pH rapidly drops, a behavior which is normally unwelcome for a buffer. In the present case this allows to have a solution which is normally almost not dissolving SiO₂ but which can be locally activated by the production of protons, e.g., by the formation of oxide. Because the protons are partially diffusing away from the interface, not all formed oxide can be dissolved at the bottom of the structure but parts remain, which leads to a porous structure. The protons which are locally lost by diffusion are then consumed for dissolving the outer part of the porous layer. To some extent, the proposed mechanism exhibits common features with pitting corrosion in metals²² (localized agglomeration of protons promoting local dissolution), though other aspects present in metals are clearly absent here (as an ultrapure material, silicon has no inclusions, etc., as passivity breakdown spots).

The images of the 15 V samples show that the porous oxide does not form regular elongated pores like, e.g., mesoporous silicon, though, of course, it remains a porous material. While substrate properties (e.g., doping concentration and orientation) have major effects on porous silicon, here they are practically of no influence on the morphology. The current limiting mechanisms are also clearly distinct (space-charge region limitation for PS vs. transport across oxide here). Therefore, similarities in pore morphology can hardly

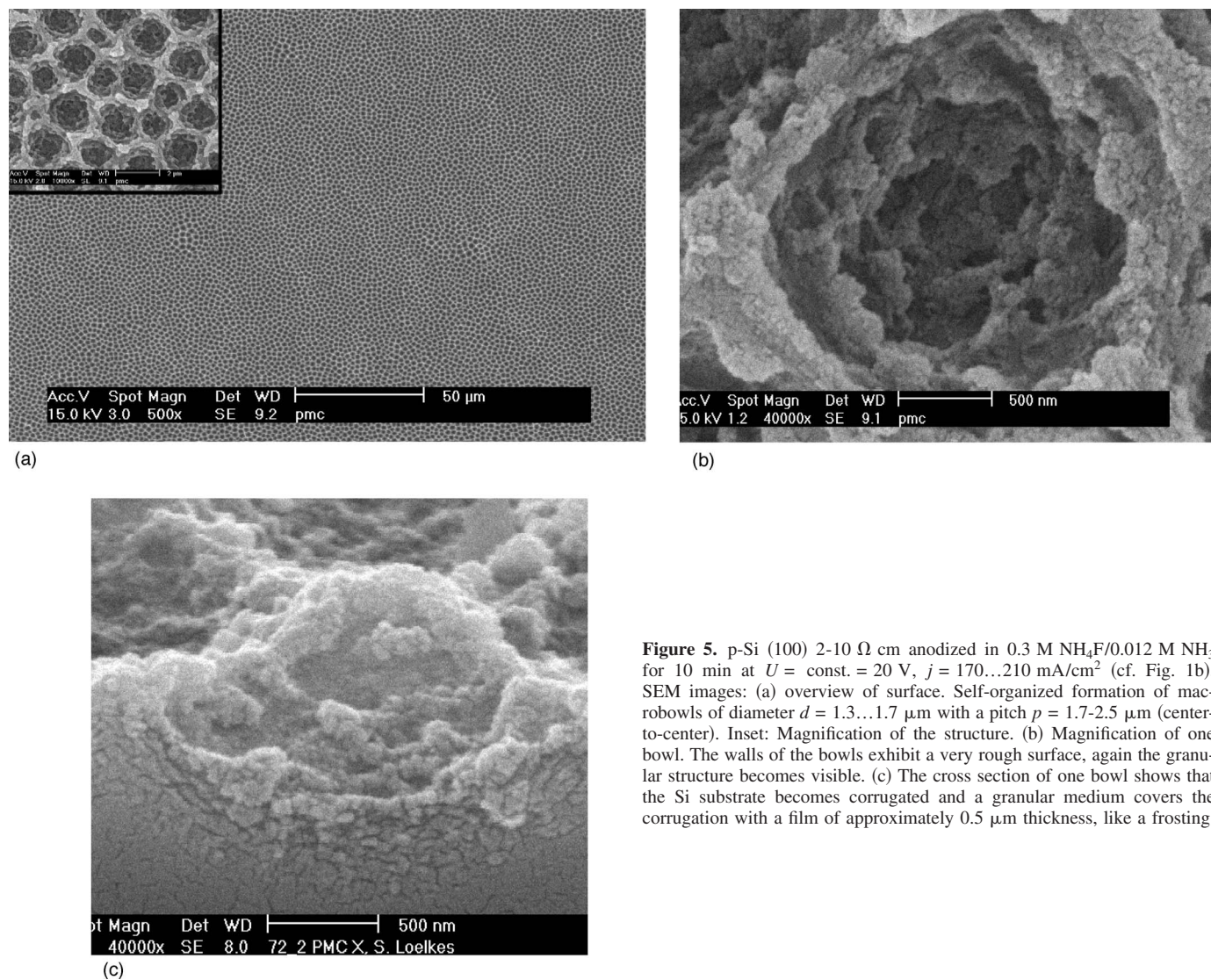


Figure 5. p-Si (100) 2-10 Ω cm anodized in 0.3 M $\text{NH}_4\text{F}/0.012$ M NH_3 for 10 min at $U = \text{const.} = 20$ V, $j = 170\text{--}210$ mA/cm² (cf. Fig. 1b), SEM images: (a) overview of surface. Self-organized formation of macrobowls of diameter $d = 1.3\text{--}1.7$ μm with a pitch $p = 1.7\text{--}2.5$ μm (center-to-center). Inset: Magnification of the structure. (b) Magnification of one bowl. The walls of the bowls exhibit a very rough surface, again the granular structure becomes visible. (c) The cross section of one bowl shows that the Si substrate becomes corrugated and a granular medium covers the corrugation with a film of approximately 0.5 μm thickness, like a frosting.

be expected. Albeit covered by Au, which hinders a closer structural analysis, an examination of Fig. 2a in combination with cross sections as in Fig. 2b, suggests a granular morphology for the porous oxide. This ball-like morphology could be linked directly to earlier proposed models for the oscillatory behavior suggesting a spatially inhomogeneous current flow.¹⁴ The so-called current bursts are assumed to form semispherical bumps in the oxide, i.e., their lateral extension is similar to the thickness of the anodic oxide. If one roughly assumes an anodic oxide thickness of 1 nm per 1 V anodization voltage (e.g., taken from experimental results from Ref. 9) 15 V translates into 15 nm bumps. Under normal anodization conditions (3-8 V, acidic HF) the characteristic size would fall in the nanometer region and acidic HF rapidly dissolves anodic oxides anyhow, so that direct observation of the corresponding structures is hardly feasible. In the present case however, an electrolyte was chosen, which suppresses nearly all dissolution of anodically formed SiO_2 . Furthermore the potential is a factor of 2 to 5 higher than under normal anodization conditions, therefore leading to much larger oxide bumps.

These characteristic sizes can be compared with those given by several other authors who investigated electrochemically formed porous silica by TEM. The structural sizes in their cases were in the range of 6-13 nm,¹⁷ respectively, 4-7 nm¹⁶ at anodization potentials of $U = 6$ V, respectively, $j = 1$ mA/cm² (at strong potential oscilla-

tions with $U = 3\text{--}13$ V) which are in reasonable agreement with the present findings if one takes into account that the anodization voltage was much larger in our case.

Finally, we end up with the picture of Fig. 6. The oxide layer thickness results from a steady state between production and dissolution of the oxide. The presence of a porous layer with a high specific surface area then allows for a high overall dissolution rate thus sustaining a high current density. Furthermore, the current flowing over the interface depends more or less exponentially on the oxide thickness, as long as the oxide layer is fully insulating. At low current, like during the positive potential sweep, a relatively thick dense oxide is present, with a negligible amount of porous oxide (cf. Fig. 6a). As the current is much higher on the upper branch of the I - V curve, the dense oxide is somewhat thinner (cf. Fig. 6b). Finally, since the dissolution of the outer part of the porous layer takes place in a weakly alkaline solution, the porous skeleton structure is chemically dissolved much more slowly than in the acidic case, i.e., the thickness of the porous oxide can get much thicker.¹⁵

Unlike previous findings^{15,16} the macrostructures in these experiments show a very narrow size distribution, and they tend to self-arrange in a (as yet polycrystalline) more or less hexagonal lattice. The underlying substrate does not influence the ordering or the structural sizes, which was checked with various dopings

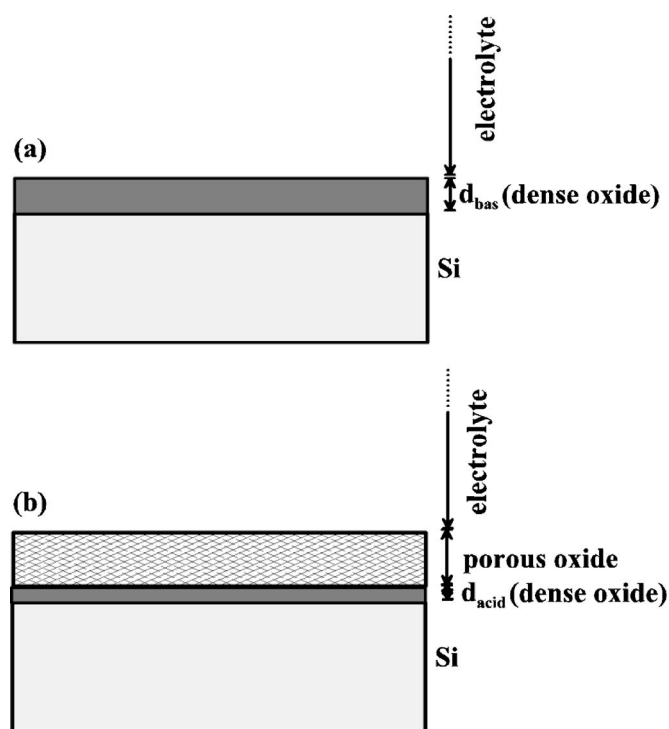


Figure 6. Interface structure in (a) the weakly alkaline case (lower branch of the I - V curve); (b) the locally acidic case (upper branch of the I - V curve).

(5-25 m Ω cm, 0.7-1.3 Ω cm, 3-6 Ω cm, 1-15 Ω cm, 30-70 Ω cm) and substrate orientations, (111) and (100). What does change the structural properties of the macrostructures is the chemistry (NH_4F concentration, rotation rate), as preliminary ongoing experiments have shown.^{19,23} From the Levich theory²⁴ the diffusion limitation induced by using a RDE with a speed of 1500 rpm leads to a diffusion-controlled electrolyte depth in front of the electrode of approximately 20 μm . This length is significantly larger than the characteristic size of the macrostructures, typically around 1-2 μm . On the other hand, the layers exhibit a granular structure similar to that of Fig. 2a, with a typical characteristic size of a few tens of nanometers. It is then likely that the length scale of the macrostructure is determined by a combination between these two effects, or is associated with an additional effect. Here the already mentioned water electrolysis could be invoked again, but this has to be investigated further.

Conclusions

We reported on the anodization of silicon under high potential in fluoride media, in particular beyond the standard regime of electrochemical oscillations. By using weakly alkaline buffered fluoride media, oxide dissolution was strongly suppressed. This leads to a huge hysteresis in the voltammogram of the system between 10 and

20 V, most probably due to an acidification in the vicinity of the electrode. We were able to reveal by optical reflectance measurements and SEM imaging that the anodic oxide layers formed under potentiostatic conditions are porous and consist of granular SiO_2 for potentials between 10 and 15 V. For anodization potentials above 15 V, well-defined macrostructures were found with a high level of self-organization. Their formation as well as the characteristic sizes were found to be strongly determined by the electrolyte composition while the underlying semiconductor substrate is not crucially guiding their development.

Acknowledgments

The authors thank Daniel Caldemaison (LMS, Ecole Polytechnique, France) for generous support with the SEM. S.F. acknowledges funding via an EU-Marie-Curie Training fellowship under HPMT-CT-2001-00328 and the DFG priority program 1113 Photonic Crystals FO 258/5-1 and 2.

Christian-Albrechts-Universität zu Kiel assisted in meeting the publication costs of this article.

References

1. H. Miyata, T. Suzuki, A. Fukuoka, T. Sawada, M. Watanabe, T. Noma, K. Takada, T. Mukaide, and K. Kuroda, *Nat. Mater.*, **3**, 651 (2004).
2. F. Keller, M. S. Hunter, and D. L. Robinson, *J. Electrochem. Soc.*, **100**, 411 (1953).
3. H. Masuda and F. Fukuda, *Science*, **268**, 1466 (1995).
4. O. Jessensky, F. Müller, and U. Gösele, *J. Electrochem. Soc.*, **145**, 3735 (1998).
5. R. Beranek, H. Hildebrand, and P. Schmuki, *Electrochem. Solid-State Lett.*, **6**, B12 (2003).
6. J. Choi, R. B. Wehrspohn, J. Lee, and U. Gösele, *Electrochim. Acta*, **49**, 2645 (2004).
7. X. G. Zhang, *Electrochemistry of Silicon and Its Oxide*, Kluwer Academic-Plenum Publishers, New York (2001).
8. V. Lehmann, *Electrochemistry of Silicon*, Wiley-VCH, Weinheim (2002).
9. J.-N. Chazalviel, C. da Fonseca, and F. Ozanam, *J. Electrochem. Soc.*, **145**, 964 (1998).
10. F. Ozanam, J.-N. Chazalviel, A. Radi, and M. Etman, *J. Electrochem. Soc.*, **139**, 2491 (1992).
11. J.-N. Chazalviel and F. Ozanam, *J. Electrochem. Soc.*, **139**, 2501 (1992).
12. H.-J. Lewerenz and M. Aggour, *J. Electroanal. Chem.*, **351**, 159 (1993).
13. V. Lehmann, *J. Electrochem. Soc.*, **143**, 1313 (1996).
14. J. Carstensen, R. Prange, and H. Föll, *J. Electrochem. Soc.*, **146**, 1134 (1999).
15. M. Lharch, M. Aggour, J.-N. Chazalviel, and F. Ozanam, *J. Electrochem. Soc.*, **149**, C250 (2002).
16. V. P. Parkhutik, E. Matveeva, R. Perez, J. Alamo, and D. Beltrán, *Mater. Sci. Eng., B*, **69-70**, 553 (2000).
17. M. Aggour, M. Giersig, and H.-J. Lewerenz, *J. Electroanal. Chem.*, **383**, 67 (1995).
18. M. Lharch, J.-N. Chazalviel, F. Ozanam, M. Aggour, and R. B. Wehrspohn, *Phys. Status Solidi A*, **197**, 39 (2003).
19. J.-N. Chazalviel, F. Ozanam, M. Lharch, J. Choi, and R. B. Wehrspohn, Abstract 2725, The Electrochemical Society Meeting Abstracts, Vol. 2003-1, Paris, France, April 27-May 2, 2003.
20. J.-N. Chazalviel, M. Etman, and F. Ozanam, *J. Electroanal. Chem. Interfacial Electrochem.*, **297**, 533 (1991).
21. <http://www.mtheiss.com>
22. G. S. Frankel, in *Pits and Pores: Formation, Properties and Significance for Advanced Luminescent Materials*, P. Schmuki, D. J. Lockwood, H. Isaacs, and A. Biesy, Editors, PV 97-7, p. 1, The Electrochemical Society Proceedings Series, Pennington, NJ (1997).
23. Unpublished results.
24. A. J. Bard and L. R. Faulkner, *Electrochemical Methods*, John Wiley & Sons, New York (1980).